Chapter 1

Modelling InSb Czochralski Growth

Tark Bouhennache[1], Leslie Fairbairn[2], Ian Frigaard[3], Joe Ho[4], Alex Hodge[5], Huaxiong Huang[6], Mahtab Kamali[7], Mehdi H. K. Kharrazi[3], Namyong Lee[8], Randy LeVeque[4], Margaret Liang[3], Shuqing Liang[6], Tatiana Marquez-Lago[2], Allan Majdanac[2], W. F. Micklethwaite[9], Matthias Mück[10], Tim Myers[11], Ali Rasekh[3], James Rossmanith[4], Ali Sanaie-Fard[3], John Stockie[12], Rex Westbrook[13], JF Williams[14], Jill Zarestky[15].

Report prepared by C. Sean Bohun[16].

1.1   Introduction

The dominant technique for producing large defect free crystals is known as the Czochralski method. Developed in 1916 by Jan Czochralski as a method of producing crystals of rare metals, this method is now used to produce most of the semiconductor wafers in the electronics industry.

The method begins with a crucible loaded with starting material (polycrystalline indium antimonide) and a seed crystal on which the growth of a single crystalline ingot is initiated. Once the starting material is melted to the correct consistency, a seed crystal is lowered on a pull rod until the tip of the seed crystal just penetrates the molten surface. At this point, the seed crystal and the crucible containing the molten starting material are counter-rotated and the temperature is adjusted until a meniscus is supported. As the pull rod is rotated, the seed crystal is slowly withdrawn from the melt developing a single crystal. By carefully controlling the temperatures and rotation rates of the crucible and the rod, a precise diameter of the resulting crystal can be maintained. This process is illustrated in Figure 1.1.

A common problem of using the Czochralski technique is that defects begin to appear in the crystal once the diameter of the crystal exceeds some critical value. The main objective of this study is to attempt to understand this phenomena by modelling the process mathematically. Hopefully, the model can also be used to design growth procedures that produce crystals without defects even when the diameters are greater than the critical values

---

[1]UCLA
[2]Simon Fraser University
[3]University of British Columbia
[4]University of Washington
[5]University of Victoria
[6]York University
[7]Concordia University
[8]Minnesota State University
[9]Firebird Semiconductors
[10]University of Toronto
[11]University of Cape Town
[12]University of New Brunswick
[13]University of Calgary
[14]University of Bath
[15]University of Texas, Austin
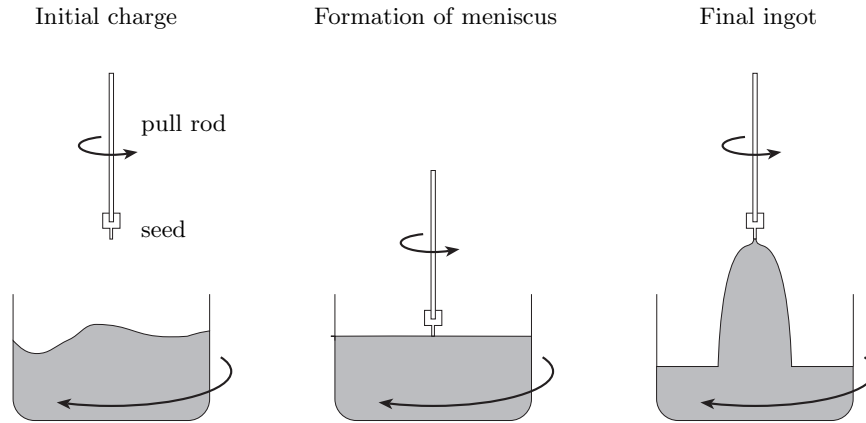[16]Pennsylvania State University

Figure 1.1: The Czochralski crystal pulling technique.

observed under current pull conditions. As indium antimonide (InSb) is used as an infrared detector, being able to manufacture large diameter crystals would have an immediate impact in industry.

The whole growing assembly is maintained in an envelope that permits the control of the ambient gas and enables the crystal to be observed visually. In the case of InSb, the ambient gas is hydrogen to ensure the reduction of any InOx compounds that may be produced. This addition of hydrogen necessitates additional complications to the growth procedure. Namely, i) the high heat losses due to the fluidity of the hydrogen and ii) the avoidance of any oxygen to avoid explosions!

Many aspects of this problem have been investigated to gain a greater insight of the physical processes involved. We begin with the heat problem first as a one dimensional model in Section 1.4 and then extending to a second dimension in Section 1.5. This analysis indicates that the temperature of the gas surrounding the crystal has a major impact on both the thermal stress experienced by the crystal and the shape of the crystal/melt interface. In contrast, variations in the heat flux from the melt have much less of an effect. For completeness the temperature profile of the crucible is also determined in Section 1.7 by neglecting the convection of the liquid InSb.

Having investigated the temperature profiles, the analysis focuses on the behaviour of the fluid in Section 1.8. Scaling arguments are used to estimate the thickness of the various boundary layers and explain the main flow patterns that are experimentally observed.

In Section 1.9 the shape of the meniscus is determined for various rotation rates. The height of the meniscus above the surface of the fluid is about 0.3 mm irrespective of the rotation rate. However, at a rotation rate of 10 rpm, the height of triple point drops about 0.15 mm from its stationary value. This analysis shows that the shape of the meniscus is relatively invariant at least at low rotation rates yet the actual vertical position of the meniscus changes readily with the rate of rotation.

After analyzing the fluid flow patterns, a model is developed in Section 1.10 for the height of the melt as a function of time. This indicates that for a crystal of constant radius the proportion of the effective pull rate due to the falling fluid level remains essentially constant over the complete growing time of the crystal. This no longer remains true if the radius of the crystal is allowed to increase at a constant rate.

1.2   Mathematical Model: Heat Flow

We begin by describing in some detail the mathematical model of the heat flow in the crystal, melt and gas assuming axial symmetry. This model will later be simplified but for now we suppose that the material, in both the solid and liquid states, cools by radiation. In the Czochralski process, the liquid is drawn up, cools to the solidification temperature, and solidifies. As a result the governing equation is

$$\frac{\partial T}{\partial t} + \nabla \cdot (\vec{v}\,T) = \frac{1}{\rho c} \nabla \cdot (k \nabla T) \tag{1.1}$$

where T denotes temperature, $\vec{v}$ velocity, ρ density, c specific heat, and k thermal conductivity. This model assumes that the fluid shear does not dissipate enough energy to heat up the liquid significantly. By fixing the coordinate system to the surface of the liquid, the velocity in the solid phase, v_p, is the sum of the crystal pull rate and the rate at which the fluid level drops in the crucible. In the melt, the fluid is assumed to be incompressible and as such the fluid velocity, v_l, satisfies $\nabla \cdot \vec{v}_f = 0$.

Let the melt/gas and crystal/gas interfaces be denoted by the surfaces $z = f_l(r, t)$ and $z = f_s(r, t)$ respectively. The normal component of the heat flux must be continuous at these surfaces. Therefore, assuming that the heat is lost through convection and radiation, this gives the boundary condition

$$-k\frac{\partial T}{\partial \mathbf{n}} = h(T - T_g) + \epsilon\sigma(T^4 - T_a^4). \tag{1.2}$$

For this expression $\mathbf{n}$ denotes the outward normal of the interface, h the heat transfer coefficient, ϵ the emittance, σ the Stefan-Boltzmann constant, T_g is the gas temperature, and T_a the ambient temperature.

The crystal/melt interface, $z = S(r, t)$, is a free boundary. At this interface

$$T = T_F \qquad \text{on} \qquad z = S(r, t) \tag{1.3}$$

where T_F is the freezing temperature and

$$\rho_s L\left(\frac{\partial S}{\partial t} - v_p\right) = \left[-k\frac{\partial T}{\partial \mathbf{n}}\right]_s^l = k_s\left(\frac{\partial T_s}{\partial z} - \frac{\partial T_s}{\partial r}\frac{\partial S}{\partial r}\right) - k_l\left(\frac{\partial T_l}{\partial z} - \frac{\partial T_l}{\partial r}\frac{\partial S}{\partial r}\right). \tag{1.4}$$

This latter condition equates the heat lost in the phase transition from liquid to solid (L per unit mass) to the net heat flux accumulating at the interface. Since InSb expands on freezing there is either a net flow of InSb away from $z = S$ or the surface of the crystal must rise. Other boundary conditions include a regularity condition at $r = 0$, an applied heat flux of Q_{app} in the crucible and a heat flux Q_{lost} lost out the top of the crystal. Figure 1.2 illustrates the geometry and summarizes the equations and boundary conditions in the crystal, melt and crucible. These problems are specifically dealt with in Sections 1.4, 1.5 and 1.7.

1.3 Nondimensionalization: Heat Flow

To identify the dimensionless parameters in the heat problem and to determine the relative importance of the various terms we set

$$r^* = r/l_r, \qquad S^* = S/l_r, \qquad z^* = z/l_z, \qquad t^* = t/\tau,$$

$$v_p^* = v_p/v_o, \qquad T^* = \frac{T - T_a}{T_F - T_a}$$

where l_r, l_z are the characteristic lengths, τ and v_o are the time and velocity scales, and $T_F - T_a$ is the representative temperature scale. In terms of these variables equation (1.1) in the crystal becomes

$$\frac{\rho_s c_s l_z^2}{k_s \tau}\left(\frac{\partial T^*}{\partial t^*} + \frac{v_o \tau}{l_z}v_p^*\frac{\partial T^*}{\partial z^*}\right) = \frac{\partial^2 T^*}{\partial z^{*2}} + \frac{l_z^2}{l_r^2}\frac{1}{r^*}\frac{\partial}{\partial r^*}\left(r^*\frac{\partial T^*}{\partial r^*}\right)$$

while the Stefan equation yields

$$\frac{\rho_s L l_z l_r}{k_s(T_F - T_a)\tau}\left(\frac{\partial S^*}{\partial t^*} - \frac{v_o \tau}{l_r}v_p^*\right) = \left(\frac{\partial T_s^*}{\partial z^*} - \frac{l_z}{l_r}\frac{\partial T_s^*}{\partial r^*}\frac{\partial S^*}{\partial r^*}\right) - \frac{k_l}{k_s}\left(\frac{\partial T_l^*}{\partial z^*} - \frac{l_z}{l_r}\frac{\partial T_l^*}{\partial r^*}\frac{\partial S^*}{\partial r^*}\right).$$

Denoting $\delta = l_r/l_z$, $\tau = l_z/v_o$, $\text{Pe} = v_o l_z \rho_s c_s/k_s$, the Péclet number based on the length in the z direction, and dropping the asterisks results in the expression

$$\text{Pe}\left(\frac{\partial T}{\partial t} + v_p\frac{\partial T}{\partial z}\right) = \frac{\partial^2 T}{\partial z^2} + \frac{1}{\delta^2}\frac{1}{r}\frac{\partial}{\partial r}\left(r\frac{\partial T}{\partial r}\right) \tag{1.5}$$

Figure 1.2: Summary of the equations, geometry and boundary conditions. The z direction is greatly exaggerated for clarity in that the interface $z = S(r,t)$ is shown in Section 1.9 to lie very close to the line $z = 0$. See Section 1.7 for an analysis of the heat in the crucible region.

and the Stefan condition becomes

$$\delta \frac{\partial S}{\partial t} = v_p + \frac{k_s(T_F - T_a)}{\rho_s L v_o l_z}\left[\left(\frac{\partial T_s}{\partial z} - \frac{k_l}{k_s}\frac{\partial T_l}{\partial z}\right) - \frac{1}{\delta}\left(\frac{\partial T_s}{\partial r}\frac{\partial S}{\partial r} - \frac{k_l}{k_s}\frac{\partial T_l}{\partial r}\frac{\partial S}{\partial r}\right)\right]. \tag{1.6}$$

Ignoring the effects of radiation, the boundary conditions at $r = 0$ and $r = 1$ are given by

$$\frac{\partial T}{\partial r}(0, z) = 0, \qquad \frac{\partial T}{\partial r}(1, z) = -\gamma[T - T_g(1, z)] \tag{1.7}$$

where $\gamma = hl_r/k_s$ from expression (1.2), $T_g(1)$ is the nondimensional gas temperature near the crystal surface, and for simplicity we have neglected the heat loss due to radiation.

As typical growth parameters for InSb we take $\rho_s L = 1.3 \times 10^9$ J m^{-3}, $T_F = 798.4$ K, $T_a \simeq 300$ K, $k_l = 9.23$ J m^{-1}s^{-1}K^{-1}, $k_s = 4.57$ J m^{-1}s^{-1}K^{-1}, $\rho_l c_l = 1.7 \times 10^6$ J m^{-3}K^{-1}, $\rho_s c_s = 1.5 \times 10^6$ J m^{-3}K^{-1}, $\rho_l = 6.47 \times 10^3$ kg m^{-3}, $\rho_s = 5.64 \times 10^3$ kg m^{-3}, $l_r = 0.03$ m, $h = 10$ J m^{-2}s^{-1}K^{-1}. With this choice of parameters

$$v_o l_z = 1.75 \times 10^{-6}, \qquad \text{Pe} = 9850\delta v_o, \qquad \gamma = 6.56 \times 10^{-2}$$

where the first parameter is determined by setting the coefficient in the Stefan equation to one. This condition connects the aspect ratio and the pull rate through $\delta = 1.71 \times 10^4 v_o$. Typical pull rates range from 0.1-100 mm hr^{-1} or about 10^{-8}-10^{-5} m s^{-1}. Consequently Pe ≤ 0.02 and the left hand side of (1.5) may be neglected.

For the numerical simulations, the temperature of the gas, $T_g(z)$, was given an exponential behaviour. In non dimensionalized form

$$T_g(z) = T_{\min} + (T_{\max} - T_{\min})e^{-\lambda z}, \qquad \lambda = 0.15, T_{\min} = 0.5, T_{\max} = 0.9. \tag{1.8}$$

A crude estimate for the fluid heat flux $k_l \partial T_l / \partial z \simeq k_l \Delta T_l / \Delta z$ where Δz is the width of the fluid boundary layer and $\Delta T = T_{\text{crucible}} - T_{\text{melt}}$. Details on how Δz is determined can be found in Section 1.8.2. In the case of InSb this gives $k_l \partial T_l / \partial z \simeq -50 k_l \simeq -450$ W m^{-2}.

Converting from the non dimensionalized values back into their dimensional versions is straightforward. Taking the non dimensionalized uniform pull rate, $v_p^* = 1$ yields

$$v_o = \frac{k_s(T_F - T_a)}{\rho_s L l_z}, \qquad \frac{\partial S}{\partial t} - v_p = v_o \left(\frac{\partial T*}{\partial z*} - \frac{k_l}{k_s} \frac{\partial T*}{\partial r*} \right)$$

and, $T = T_a + (T_F - T_a)T^*$. The fixed uniform pull rate is an artifact of choosing the coefficient in expression (1.6) to be unity and could be changed with the addition of another parameter. Finally, since the system is encapsulated, the ambient temperature is probably much higher that $T_a = 300$ K. Increasing T_a will result in a corresponding drop in the value of v_p.

1.4   First Steps: A 1D Temperature Model

For any fixed height z the average of the temperature across the crystal radius is given by

$$\overline{T}(z) = 2 \int_0^1 T(r, z) \, r \, dr$$

where we have used the non dimensionalized coordinates. Applying this averaging technique to equations (1.3), (1.5) and (1.7) we obtain the second order linear nonhomgeneous boundary value problem

$$\frac{d^2\overline{T}}{dz^2} = -\frac{2\gamma}{\delta^2}[\overline{T} - T_g(z)], \qquad \overline{T}(0) = 1, \; \frac{d\overline{T}}{dz}(1) = -\frac{\gamma}{\delta}[\overline{T}(1) - T_g(1)] \tag{1.9}$$

where $T_g(z)$ is given by (1.8) and $\delta = l_r/l_z = 1/3$. The growth of the crystal/melt interface is governed by the Stefan condition (1.6) and by assuming that the slope of the interface is small, $|\partial S/\partial r| \ll 1$, one obtains

$$\delta \frac{\partial S}{\partial t} = v_p + \frac{\partial T_s}{\partial z} - \frac{k_l}{k_s} \frac{\partial T_l}{\partial z}. \tag{1.10}$$

With this averaging method, $T_s = \overline{T}(0)$ while the value for $k_l \partial T_l / \partial z \simeq -450$ W m^{-2}.

Expression (1.9) was solved using a shooting method starting at $z = 1$ and shooting towards $z = 0$. The Robin condition, $d\overline{T}/dz(1) = -(\gamma/\delta)[\overline{T}(1) - T_g(1)]$ precluded starting at $z = 0$. In detail, the temperature $\overline{T}(1)$ was assumed and $d\overline{T}/dz(1)$ is given by the Robin condition. The next choice for $\overline{T}(1)$ depends on the value of $\overline{T}(0)$, the method converging once $\overline{T}(0) = 1$. Solving (1.9) for $\overline{T}(z)$ gives the decreasing temperature profile shown on the left of Figure 1.3. The right side of the illustration is the temperature dependence of the gas, $T_g(z)$. In this case $T_F - T_g(0) = 80$ K in dimensionalized units and the interface velocity from uniform, $v_p = 70$ mm hr^{-1}, is $\partial S/\partial t - v_p = -29.6$ mm hr^{-1}. Figure 1.4 illustrates the relative velocity as $T_F - T_g(0)$ varies from 80 K to 400 K. As expected, increasing $T_F - T_g(0)$ increases the speed of the interface.

1.5   2D Temperature Distribution of the Crystal

For the two dimensional problem we return to expression (1.5) and make the standard ansatz
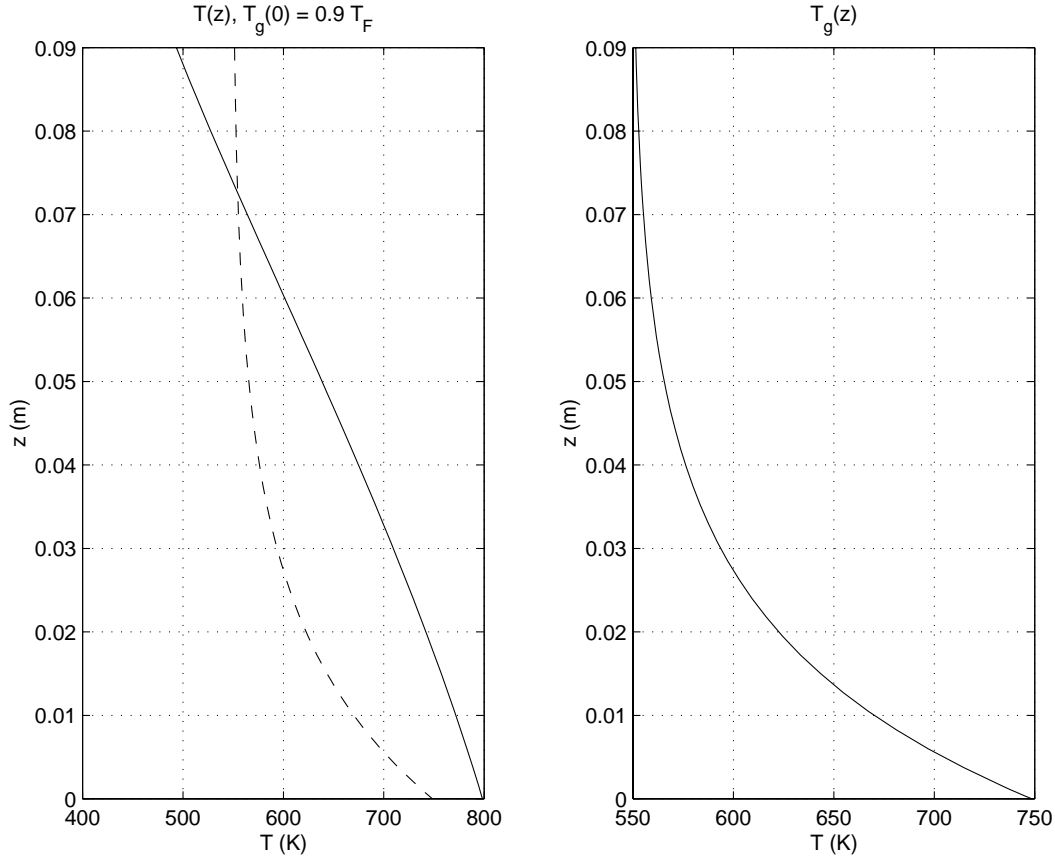
$$T(r, z) = T_0 + \delta T_1 + \delta^2 T_2 + \cdots.$$

Figure 1.3: The left graph shows the average temperature $\overline{T}(z)$ over the length of the crystal with the temperature of the gas $T_g(z)$ overlaid for comparison. On the right is just the temperature of the gas. The uniform interface velocity is $v_p = 70$ mm hr^{-1} and the deviation from uniform, $\partial S/\partial t - v_p = -29.6$ mm hr^{-1}.

This implies that T_0 satisfies

$$\frac{1}{r}\frac{\partial}{\partial r}\left(r\frac{\partial T_0}{\partial r}\right) = 0, \qquad \left.\frac{\partial T_0}{\partial r}\right|_{r=0} = 0, \qquad \left.\frac{\partial T_0}{\partial r}\right|_{r=1} = -\gamma[T_0 - T_g(z)]$$

giving $T_0 = T_g(z)$. Continuing in this fashion we find to $O(\delta^2)$ that

$$T(r,z) = T_g(z) + \delta^2\left(1 - r^2 + \frac{2}{\gamma}\right)\frac{T_g''(z)}{4}. \tag{1.11}$$

A difficulty arises as $z \to 0$ where in the non dimensionalized variables we have the condition $T = 1$. It is unlikely that $T(r,0) = 1 = T_g(0)$ so that a boundary layer correction is required. For the boundary layer solution, T_{bl}, we rescale the z in expression (1.5) by δ and denote $\tilde{z} = z/\delta$. When the equations are scaled in this way T_{bl} satisfies

$$\frac{\partial^2 T_{\text{bl}}}{\partial \tilde{z}^2} + \frac{1}{r}\frac{\partial}{\partial r}\left(r\frac{\partial T_{\text{bl}}}{\partial r}\right) = 0 \tag{1.12}$$

with the boundary conditions

$$\frac{\partial T_{\text{bl}}}{\partial r}(0,\tilde{z}) = 0, \qquad \frac{\partial T_{\text{bl}}}{\partial r}(1,\tilde{z}) = -\gamma(T - T_g), \qquad T_{\text{bl}}(r,0) = 1 - T_g(0), \qquad \lim_{\tilde{z}\to\infty} T_{\text{bl}}(r,\tilde{z}) = 0. \tag{1.13}$$
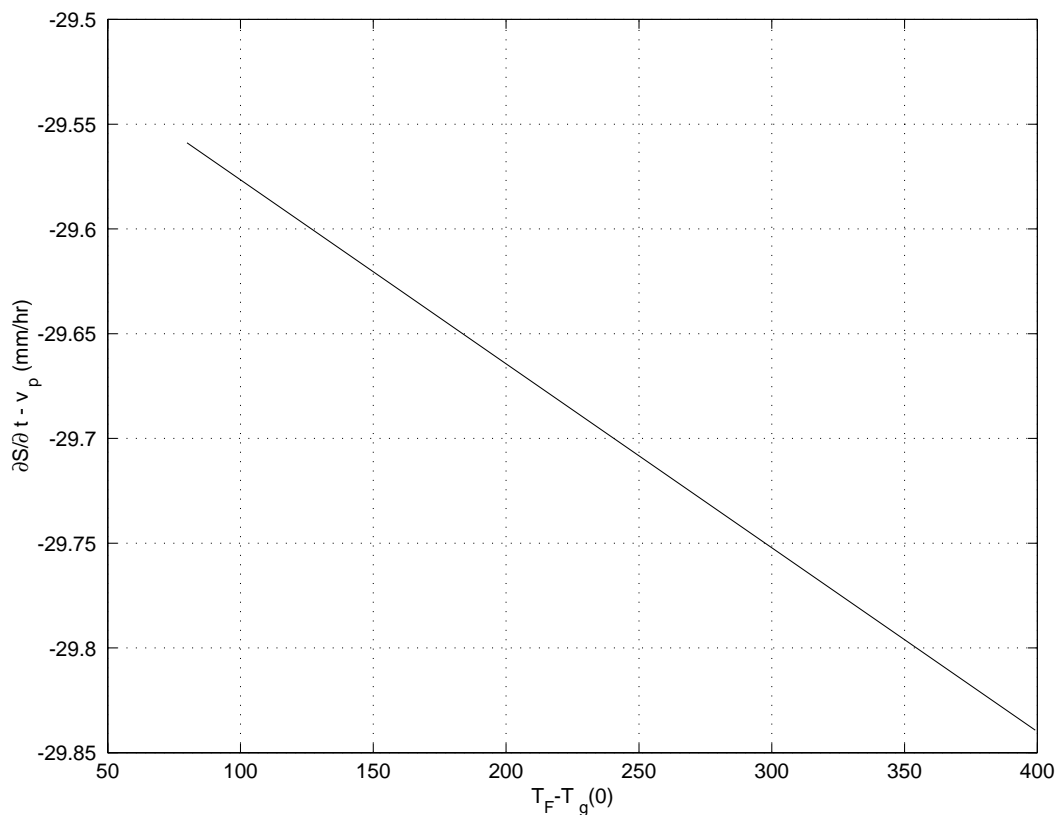
Figure 1.4: The deviation from uniform interface velocity, $\partial S/\partial t - v_p$, as a function of $T_F - T_g(0)$.

At $\tilde{z} = 0$ the condition $1 - T_g(0)$ corrects for the $T_g(0)$ from expression (1.11). Solving (1.12)-(1.13) gives to leading order in δ

$$T(r, z) = T_g(z) + T_{\mathrm{bl}}(r, z) = T_g(z) + [1 - T_g(0)] \sum_{n=0}^{\infty} \frac{2\gamma}{\gamma^2 + \zeta_n^2} \frac{J_0(\zeta_n r)}{J_0(\zeta_n)} e^{-\zeta_n z/\delta} \tag{1.14}$$

where J_0 is the zeroth order Bessel function of the first kind and the ζ_n are the zeros of $\zeta_n J_0'(\zeta_n) = -\gamma J_0(\zeta_n)$.

As with the one dimensional case, the growth of the crystal/melt interface is governed by the Stefan condition (1.10) where $\partial T_s/\partial z$ now varies with r according to expression (1.14).

For the numerical simulations, $T_g(z)$ was specified by equation (1.8) and $k_l \partial T_l/\partial z$ was varied linearly over the radial coordinate by 15% with an average value of -450 W m^{-2} as in the one dimensional case so that $k_l \partial T_l/\partial z \simeq$ -480 W m^{-2} at $r = 0$ and $k_l \partial T_l/\partial z \simeq$ -420 W m^{-2} at $r = 1$. Choosing $\delta = 1/3$ gives a uniform pull rate of $v_p = 70$ mm hr^{-1}. The corresponding two dimensional temperature profile is illustrated in Figure 1.5 and should be compared with Figure 1.3, the profile for the one dimensional case. Since the isotherms in the two dimensional situation are quite flat one would expect considerable agreement with the temperature in the one dimensional case. However, due to the difference in the boundary condition at large z, the temperature decreases with z much faster in the two dimensional case. As a result, the speed of the interface, illustrated in Figure 1.6, is about three times that predicted with the one dimensional model. The model accurately predicts that the growth rate is larger near the periphery of the crystal so that the interface is concave down. This asymmetry in the growth rate across the interface increases as $T_F - T_g(0)$ increases. At the other extreme, $T_g(0) > T_F$ the gas melts the crystal and the shape of the crystal/melt interface becomes concave up. Clearly, controlling the the temperature of the surrounding gas is critical in reducing the thermal stress within the crystal.
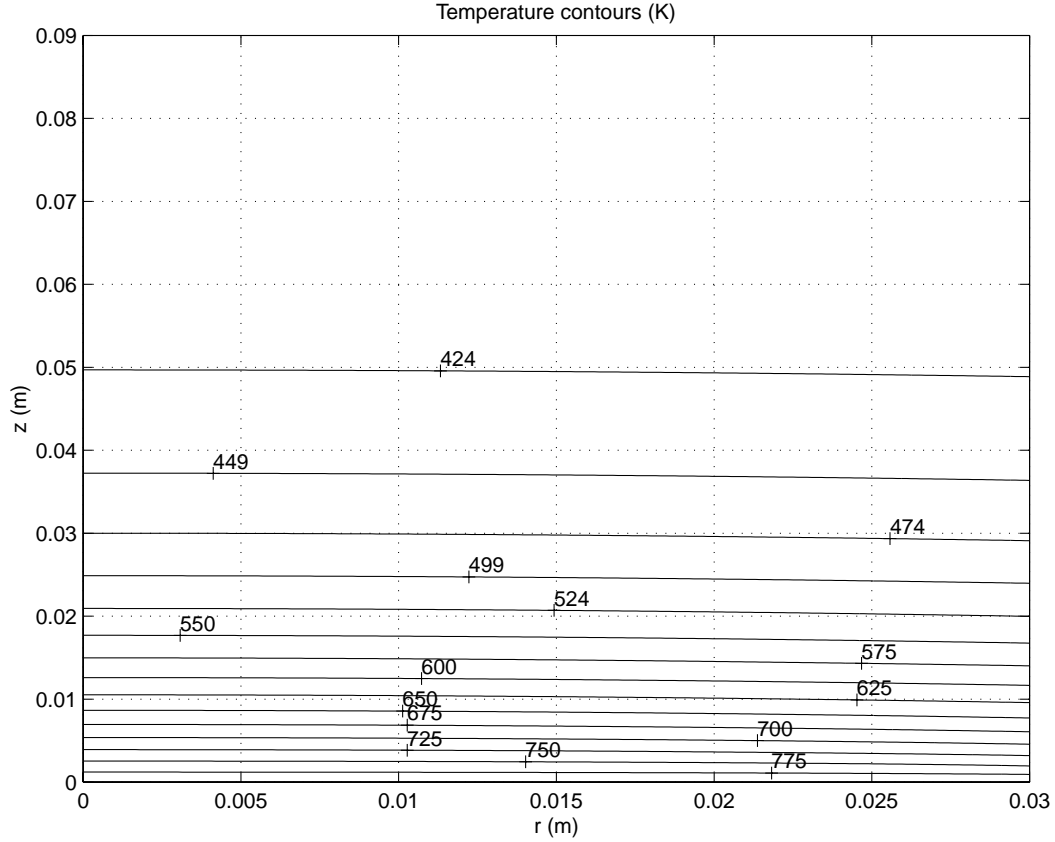
Figure 1.5: Temperature profile $T(r, z)$ in the crystal with $\delta = 1/3$.

1.6   The Thermal Stress Problem

The temperature distribution induces a thermal stress field in the crystal due to the inhomogeneities in the thermal contraction. Some analytical insight as to the source of the stress can be gained by supposing that we have a thin body, $l_r/l_z \ll 1$, and looking at the outer region where the scaling r/l_r and z/l_z is appropriate. The radial and axial displacements u and w are scaled in a similar fashion u/l_r and w/l_z. The thermal stresses are scaled by $\alpha T_F E$ where α is the thermal expansion coefficient, T_F is the melting temperature and E the Young's modulus. Under this scaling the strains are $O(1)$.

In terms of scaled variables and using the result $T = T_g(z)$ from Section 1.5 yields

$$\epsilon_r = T_g(z) + [\sigma_r - \nu(\sigma_\theta + \sigma_z)] = \frac{\partial u}{\partial r}$$

$$\epsilon_\theta = T_g(z) + [\sigma_\theta - \nu(\sigma_r + \sigma_z)] = \frac{u}{r}$$

$$\epsilon_z = T_g(z) + [\sigma_z - \nu(\sigma_r + \sigma_\theta)] = \frac{\partial w}{\partial z}$$

$$\epsilon_{rz} = (1 + \nu)\sigma_{rz} = \frac{1}{2}\left(\delta\frac{\partial u}{\partial z} + \frac{1}{\delta}\frac{\partial w}{\partial r}\right).$$
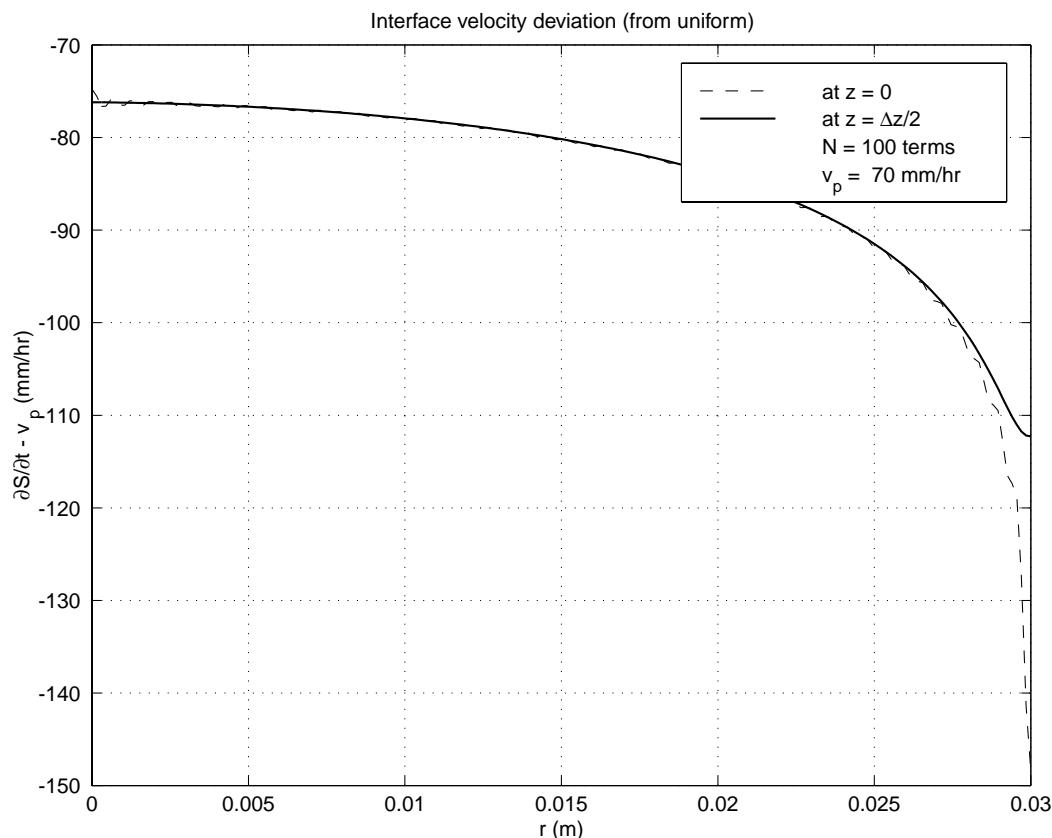
Figure 1.6: Radial dependence of the relative speed of the interface $\partial S/\partial z - v_p$ with $\delta = 1/3$. The dashed curve is the speed at $z = 0$ while the solid curve is the speed just inside the interface at $z = \Delta z/2$. Negative values indicate that the interface is growing downwards. Finally, the $N = 100$ indicates that the Bessel series solution was truncated at 100 terms.

with ν the Poisson ratio. The scaled equilibrium equations are

$$\frac{\partial}{\partial r}\sigma_r + \frac{1}{r}(\sigma_r - \sigma_\theta) + \delta\frac{\partial}{\partial z}\sigma_{rz} = 0$$

$$\frac{\partial}{\partial r}\sigma_{rz} + \frac{1}{r}\sigma_{rz} + \delta\frac{\partial}{\partial z}\sigma_z = 0.$$

As for boundary conditions, because of the axisymmetry we have the $u = 0$ and $\partial w/\partial r = 0$ at $r = 0$ while the boundary at $r = 1$ is unstressed so that $\sigma_r = \sigma_{rz} = 0$ at $r = 1$.

Making the standard ansatz $u = u^0 + \delta u^1 + \cdots$, $w = w^0 + \delta w^1 + \cdots$ and using the expression for ϵ_{rz} one has

$$2(1+\nu)\sigma_{rz} = \frac{1}{\delta}\frac{\partial w^0}{\partial r} + \frac{\partial w^1}{\partial r} + \delta\frac{\partial u^0}{\partial z} + O(\delta^2).$$

Since ϵ_{rz} is $O(1)$, $w^0 = W(z)$ and therefore $\sigma_{rz}^0 = 0$. In addition, the second equilibrium equation implies that

$$\frac{\partial}{\partial r}(r\sigma_{rz}^1) = -r\frac{\partial}{\partial z}\sigma_z^0$$

and by applying the boundary condition at $r = 1$ we have $\sigma_{rz}^1 = 0$ and $\partial\sigma_z^0/\partial z = 0$.

The relationship for u^0 comes from the first equilibrium equation which reduces to

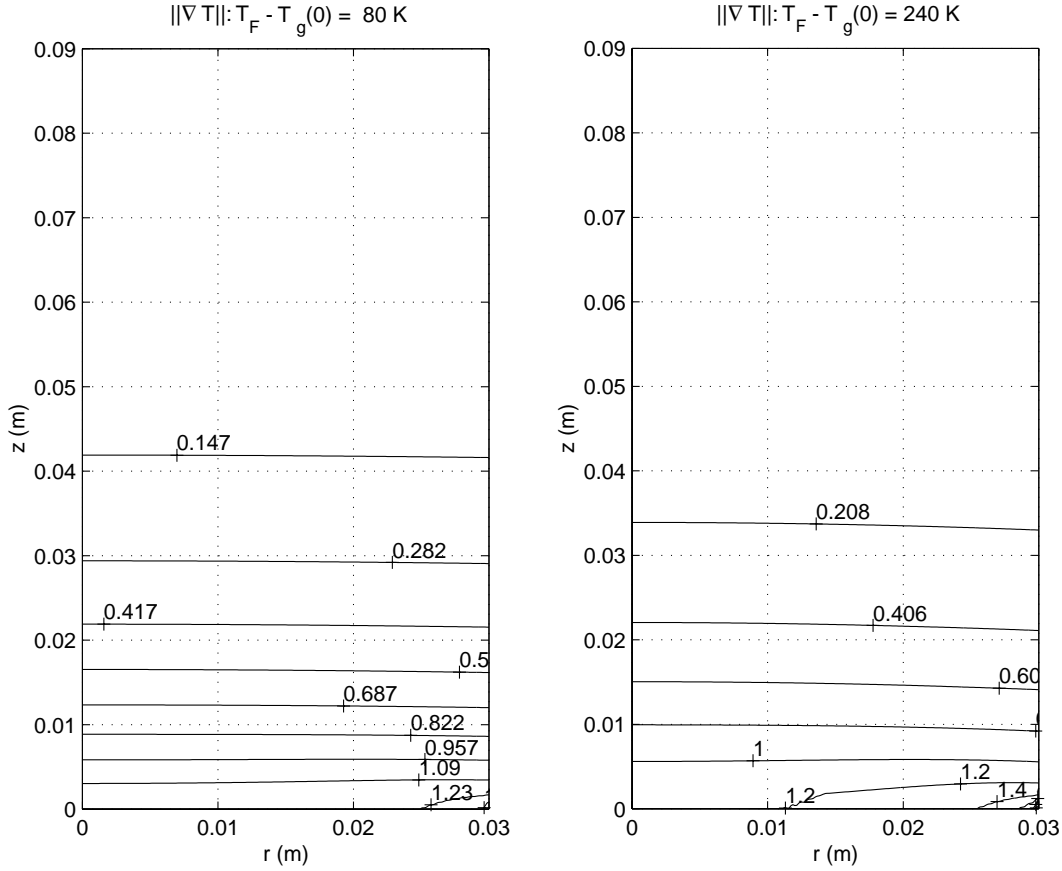$$\frac{\partial^2 u^0}{\partial r^2} + \frac{1}{r}\frac{\partial u^0}{\partial r} - \frac{1}{r^2}u^0 = 0$$

Figure 1.7: Norm of the gradient of the temperature as $T_g(0)$ varies. The figure on the left has $T_g(0) = 720$ K and the figure on the right has $T_g(0) = 560$ K.

with solution $u^0 = A(z)r$. Thus we obtain

$$\sigma_r^0 = \frac{A(z) + \nu W'(z)}{(1+\nu)(1-2\nu)} - \frac{T_g(z)}{(1-2\nu)}.$$

Using the boundary condition at $r = 1$ once again gives $\sigma_r^0 = 0$ and hence $A(z) = -\nu W'(z) + (1+\nu)T_g(z)$. In a similar fashion we obtain $\sigma_\theta^0 = 0$ and $\sigma_z^0 = W'(z) - T_g(z) = C$, a constant. If we consider the exact solution for the whole cylinder when the base of the crystal is stress free and simple equilibrium considerations give

$$\int_0^1 \sigma_z r \, dr = 0$$

at any value of z, thus we may conclude that $\sigma_z^0 = 0$ and $W'(z) = T_g(z)$.

Thermal stress will be restricted to a region within a distance l_r from the growing surface. Since these stresses, in the nondimensional case, will depend on the scaled temperature difference $1 - T_g(0)$ we expect them to be of magnitude $\alpha E[T_F - T_g(0)]$ and they will be determined by a solution of the full axisymmetric equations; a problem which appears to be analytically intractable. However it is clear that the magnitude of the stresses can be controlled by making $T_F - T_g(0)$ as small as possible. As numerical evidence of these observations Figure 1.7 displays contours for the norm of the temperature gradient as an indicator of the total stress. Figure 1.8 shows the von Mises stress produced by the temperature distribution obtained in Section 1.5. The von Mises stress is defined as

$$\sigma_e = \left[\frac{(\sigma_1 - \sigma_2)^2 + (\sigma_1 - \sigma_3)^2 + (\sigma_2 - \sigma_3)^2}{2} \right]^{1/2}$$
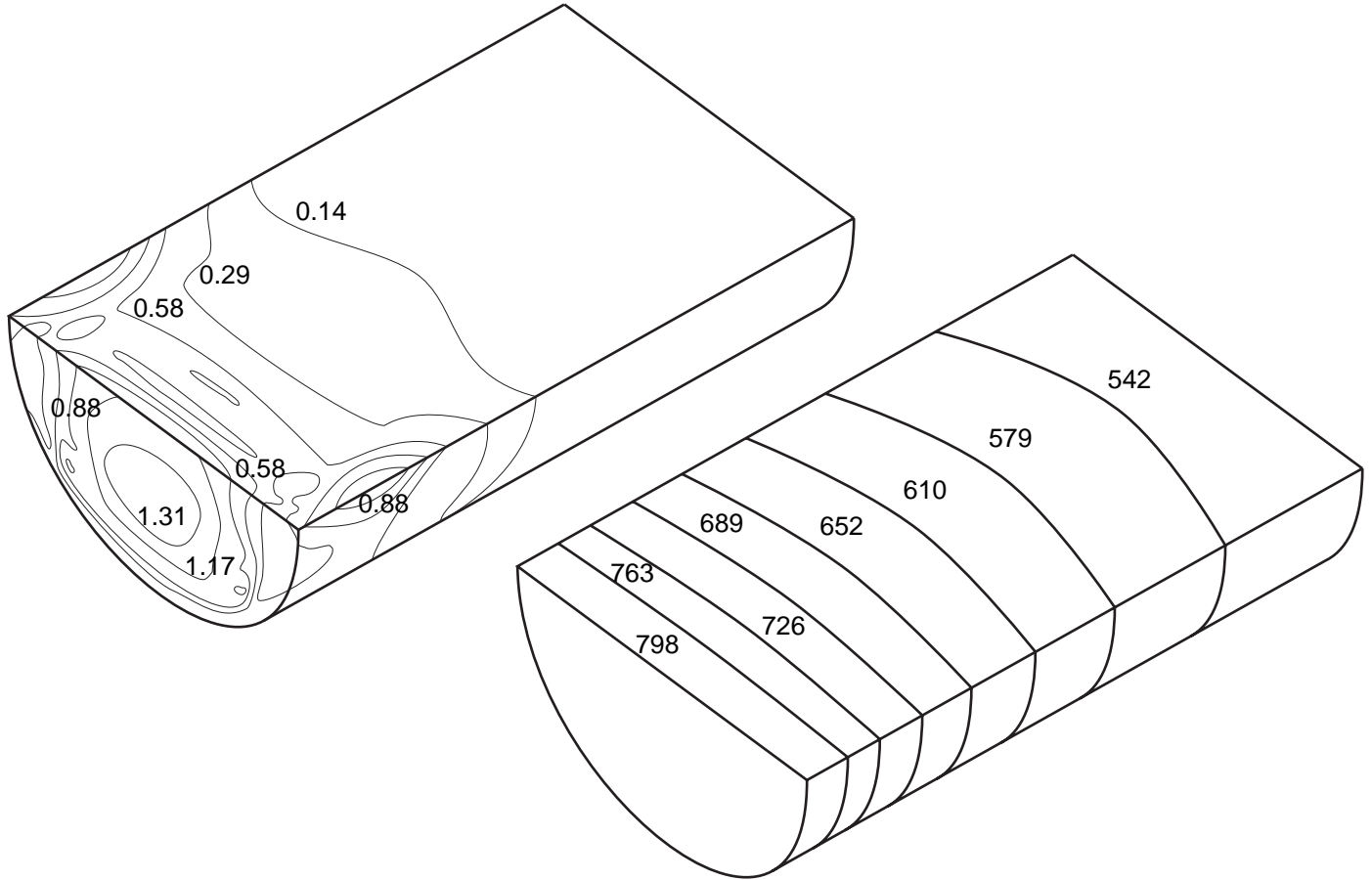
Figure 1.8: von Mises stress of an InSb crystal together with the corresponding temperature distribution.

where σ_1, σ_2 and σ_3 are the principle stresses at a given point within the crystal.

1.7 Distribution of Heat in the Crucible

For completeness we now determine the temperature profile in the crucible and the holder assuming no motion of the fluid. The isotherms will be modified by any convective flow in the crucible but as we will see in Section 1.8 this flow is practically inviscid so that the temperature will for the most part remain radially stratified. Figure 1.9 illustrates the domain and summarizes the boundary conditions. For the interior region we have liquid InSb with a thermal conductivity of $k_l = 9.23$ W m^{-1}K^{-1}. Outside of this is a thin layer of quartz, 3 mm, with a conductivity of approximately $k_q = 1.5$ W m^{-1}K^{-1} and finally surrounded by a layer of graphite with $k_g = 120$ W m^{-1}K^{-1}. It should be noted that for simplicity we have taken the thermal conductivity of each of these materials to be constant however they are actually functions of the temperature. For example, k_g varies from 150 W m^{-1}K^{-1} to 100 W m^{-1}K^{-1} as the temperature increases from 300 K to 900 K.

This problem is complicated by the involved boundary conditions. There is a regularity condition at $r = 0$ and a heat inflow at $r = 0.1$ m with an applied heat flux of about $Q_{\mathrm{app}} = 1200$ W. At $z = -0.16$ m there is heat lost due to convection with a heat transfer coefficient $h = 10$ W m^{-2}K^{-1} to the surrounding hydrogen gas at a temperature $T_{g1} = 600$ K. At the top of the melt, $z = 0$, there are two conditions. At the crystal/melt interface the temperature of the melt is the solidification temperature of the crystal. Therefore, $T = T_F = 798.4$ K for $z = 0$ and $0 \leq r \leq l_r$ with $l_r = 0.03$ m. The remainder of this boundary suffers heat loss due to convection again with a heat transfer coefficient of $h = 10$ W m^{-2}K^{-1} but in this case the surrounding gas is taken to have a temperature of about $T_{g2} = 700$ K. Two final conditions are that the temperature flux must be continuous at the
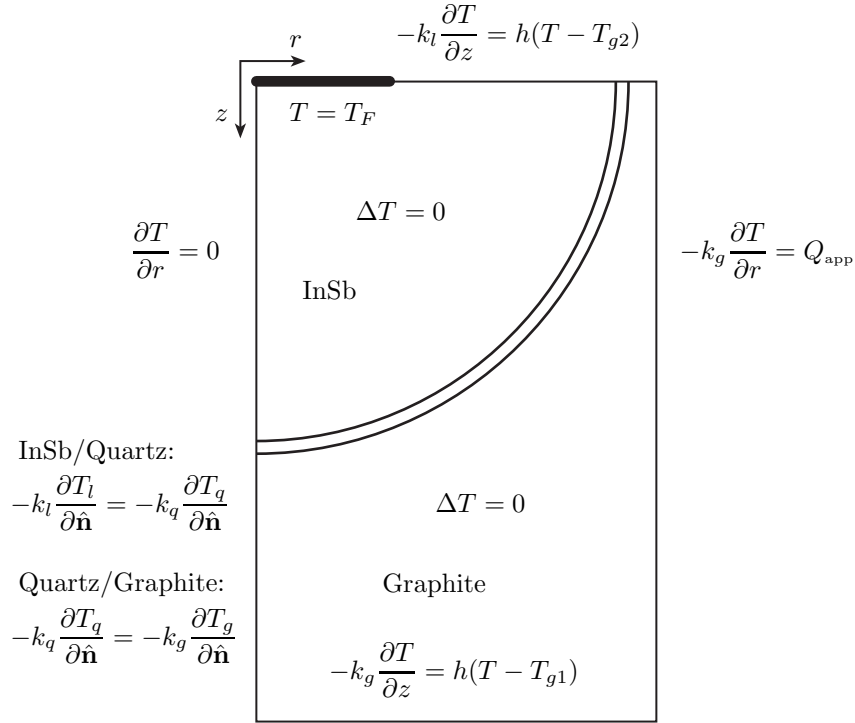
Figure 1.9: Shown here is the geometry and boundary conditions for solving the steady state heat equation in the crucible and the holder. Summarizing the parameters: $k_l = 9.23$ W m^{-1}K^{-1}, $k_q = 1.5$ W m^{-1}K^{-1}, $k_g = 120$ W m^{-1}K^{-1}, $T_F = 798.4$ K, $Q_{\text{app}} = 1200$ W, $h = 10$ W m^{-2}K^{-1}, $T_{g1} = 600$ K, $T_{g2} = 700$ K, and $l_r = 0.03$ m.

graphite/quartz and the quartz/InSb boundaries. Figure 1.10 shows the isotherms and the interesting artifact of a cold spot at the bottom of the holder at $r = 0$.

1.8 Mathematical Model: Fluid Flow

We now turn our attention to the behaviour of the fluid. The fundamental equations of the fluid motion are governed by the incompressible Navier-Stokes equations within a rotating crucible. We assume that the flow is independent of the azimuthal angle and that the variations in the fluid density can be ignored except insofar as their effect on the gravitation forces. This latter assumption is known as the Boussinesq approximation.

Consider for a moment the force on the fluid due to gravity

$$\vec{F}_g = \rho_l \vec{g} = -\rho \nabla \phi$$

where $\phi = gz$ is the gravitational potential and ρ_l is the density of the fluid. By expressing the density as a constant ρ_o and a small variation ρ_ϵ we have $\rho_l = \rho_o + \rho_\epsilon$ with $\nabla \rho_o = 0$ and

$$\vec{F}_g = -\nabla(\rho_o \phi) + \rho_\epsilon \vec{g}.$$

Redefining the pressure as $P' = P + \rho_o \phi$ gives the expression

$$-\nabla P + \vec{F}_g = -\nabla P' + \rho_\epsilon \vec{g}. \tag{1.15}$$

Since the change in density, ρ_ϵ, is for the most part a result of heating the fluid, we linearize this change in density so that $\rho_\epsilon \simeq \beta(T - T_F)$ where β is the thermal coefficient of expansion.

The fact that the crucible is rotating introduces a coriolis force and a reaction force due to the centripetal acceleration of the fluid particles. This second force can be written as a potential and combined with the
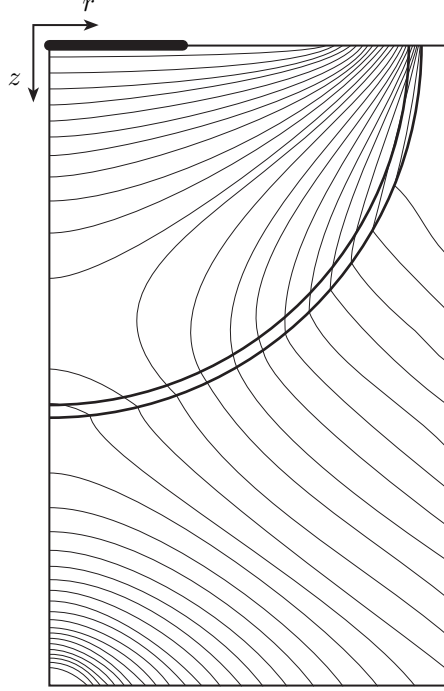
Figure 1.10: Illustrated is the temperature profile of the crucible and the holder. Note the cold spot at the base of the holder at $r = 0$. This pattern is expected to persist in the presence of the convective flow of the melt since in Section 1.8 it is shown that the fluid flow is essentially inviscid.

nonrotating gravitational potential to give

$$\phi = gz - \frac{1}{2}\omega_1^2 r^2 \tag{1.16}$$

where $-\nabla\phi$ is the measured graviational force in the accelerated frame and we have taken the rotation rate $\vec{\omega} = -\omega_1\hat{\mathbf{k}}$.

Combining (1.15), (1.16) and the azimuthal symmetry of the flow yields the following pseudo-steady incompressible Navier-Stokes equations for the fluid velocity $\vec{v}_l = \langle u_r, u_\theta, u_z \rangle$

$$u_r\frac{\partial u_r}{\partial r} + u_z\frac{\partial u_r}{\partial z} = -\frac{1}{\rho_o}\frac{\partial P'}{\partial r} - 2\omega_1 u_\theta + \nu\Delta u_r \tag{1.17}$$

$$u_r\frac{\partial u_\theta}{\partial r} + u_z\frac{\partial u_\theta}{\partial z} = 2\omega_1 u_r + \nu\Delta u_\theta \tag{1.18}$$

$$u_r\frac{\partial u_z}{\partial r} + u_z\frac{\partial u_z}{\partial z} = -\frac{1}{\rho_o}\frac{\partial P'}{\partial z} + \nu\Delta u_z - \beta g(T - T_F). \tag{1.19}$$

Although it does not appear in these expressions, the angular velocity of the crystal is taken to be $\omega_2\hat{\mathbf{k}}$ which is in the opposite direction to that of the crucible. In addition to these three equations, the fluid is incompressible and the temperature satisfies expression (1.1). Thus in component form we have

$$\frac{1}{r}\frac{\partial}{\partial r}(ru_r) + \frac{\partial}{\partial z}u_z = 0 \tag{1.20}$$

$$u_r\frac{\partial T}{\partial r} + u_z\frac{\partial T}{\partial z} = \frac{k_l}{\rho_o c_l}\Delta T. \tag{1.21}$$

Even without specifying any boundary conditions, the complexity of these five expressions precluded any detailed simulation of the flow. However, it is known by observing the melt that there exist three distinct regions
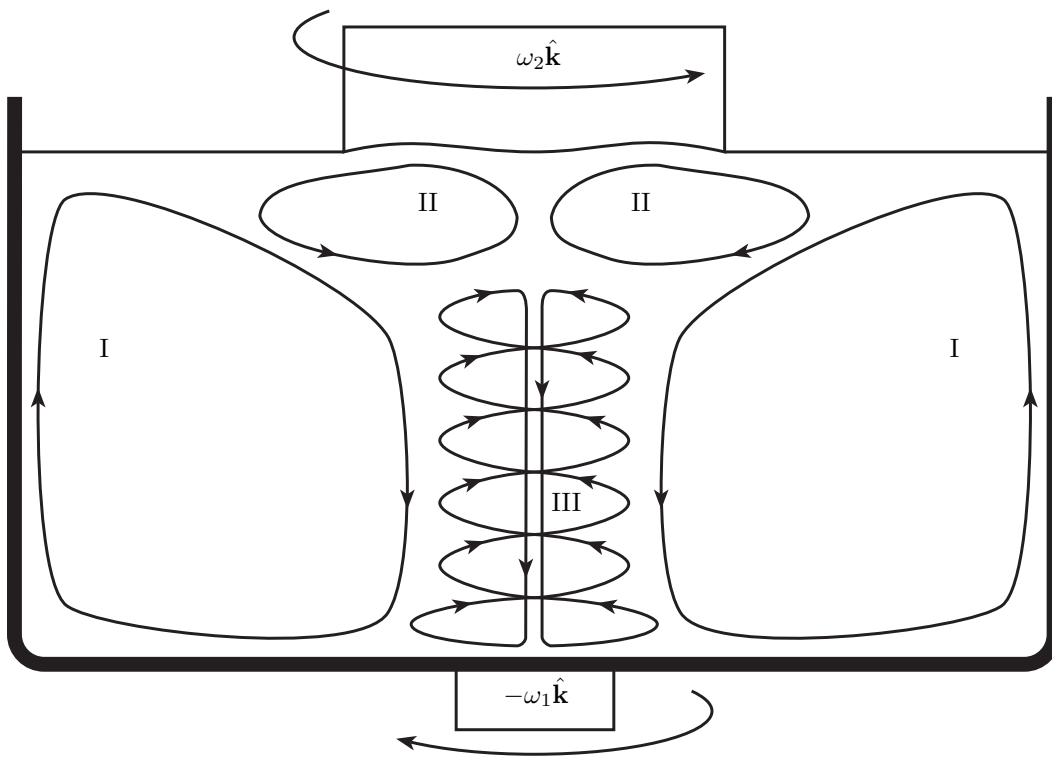
Figure 1.11: Experimentally observed flow pattern of the liquid InSb. The three major features are I: a buoyancy drive cell; II: a cell driven by Ekman pumping; III: a transient spiral.

Data	Symbol	Value
Growing Properties		
Crystal Radius	l_r	0.03 m
Crucible Radius	R_c	0.08 m
Liquid Properties		
Melting Temperature	T_F	798.4 K
Density	ρ_l	6.47×10^4 kg m^{-3}
Thermal Conductivity	k_l	9.23 W m^{-1}K^{-1}
Heat Capacity	$\rho_l c_l$	1.7×10^6 J m^{-3}K^{-1}
Thermal Diffusivity	α	5.4×10^{-6} m^{2}s^{-1}
Dynamic Viscosity	ν	3.3×10^{-7} m^{2}s^{-1}
Coefficient of Expansion	β	1×10^{-4} K^{-1}

Table 1.1: A summary of the physical parameters of liquid InSb.

of flow as depicted in Figure 1.11. Cell I is a buoyancy driven cell from expression (1.19). Cell II results from Ekman pumping and is a consequence of (1.17) and (1.18). Cell III is a complex spiral that is expected to exist at higher rotation rates.

Over the next couple subsections each of these regions are analysed using the material parameters of the liquid InSb and in preparation of this, these parameters are collected in Table 1.1.

1.8.1 Cell I

This cell is a buoyancy driven cell resulting from the upwelling of heated InSb at the outside wall of the crucible and the subsequent radial inflow as the fluid cools. By comparing the relative strengths of the inertial, buoyancy and viscosity forces on a packet of fluid the width and flow rate of this viscous boundary layer can be estimated. Let the viscous boundary layer have thickness δ_I and an upward velocity of u_I at the crucible wall. The subscript refers to the cell under consideration. For the length scale, we choose the height of the crucible which is approximately R_c. Balancing the three forces yields the expression

$$\frac{u_I^2}{R_c} \simeq \beta g(T - T_F) \simeq \frac{\nu u_I}{\delta_I^2}$$

and a little rearranging gives

$$\mathrm{Re}_I = \frac{u_I R_c}{\nu} = \mathrm{Gr}_I^{1/2}, \qquad \delta_I = \mathrm{Gr}_I^{-1/4} R_c$$

where Re_I is the Reynolds number and $\mathrm{Gr}_I = \beta g(T - T_F)R_c^3/\nu^2$ is the Grashof number. As with liquid metals, the Prandtl number $\mathrm{Pr}_I = \nu/\alpha \simeq 0.061 \ll 1$ which implies that there is a very thin viscous boundary as compared to the thermal boundary layer so that the heat flow is driven by the thermal diffusivity.

To determine whether or not there is a convective flow we compute the Rayleigh number, $\mathrm{Ra} = \mathrm{GrPr}$. If Ra exceeds a critical value (about 1100 for a free surface) then a convective flow is expected. In our case $T - T_F \simeq 30$ K so that $\mathrm{Ra}_I \simeq 2.8 \times 10^4$ and indeed we predict that there will be a buoyancy cell. This buoyancy cell is practically unavoidable in that one requires $T - T_F < 10^{-3}K$ to prevent it. Having established that there is a convective flow, the speed of the upwelling InSb is given by the relationship $v_{o,I}\delta_I \simeq \alpha$ or $v_{o,I} \simeq \alpha \mathrm{Gr}^{1/4}/R_c$. The flow rate around the cell is $Q_I = 2\pi R_c \delta_I v_{o,I} = 2\pi \alpha R_c$. Finally, in the core region the speed of the falling fluid satisfies $\pi l_r^2 v_{i,I} = 2\pi \alpha R_c$ which implies that $v_{i,I} = 2\alpha R_c/l_r^2$. Setting $T - T_F \simeq 30$ K gives $\mathrm{Gr}_I = 1.4 \times 10^8$, $\mathrm{Re}_I = 1.2 \times 10^4$, $\delta_I = 0.7$ mm, $v_{o,I} = 7.4$ mm s^{-1}, $v_{i,I} = 0.97$ mm s^{-1} and $Q_I = 2.7$ ml s^{-1}.

1.8.2   Cells II and III

The steady velocity of the rotating crystal at $z = 0$ produces a thin boundary layer at the surface. By assuming a horizontal flow at the surface, expressions (1.18) and (1.19) reduce to

$$-2\omega u_\theta + \nu \frac{\partial^2 u_r}{\partial z^2} = 0$$

$$2\omega u_r + \nu \frac{\partial^2 u_\theta}{\partial z^2} = 0$$

where $\omega = |\omega_1 - \omega_2|$ by taking into account the combined rotation of the crystal and the crucible. Letting $\vec{v}_l(z = 0) = \langle 0, v_o, 0 \rangle$ and choosing $\lim_{z \to -\infty} \vec{v}_l(z) = 0$ in the geometry of Figure 1.2 we have the solution

$$\vec{v}_l(z) = v_o e^{z/\delta_{II}} \langle \sin(z/\delta_{II}), \cos(z/\delta_{II}), 0 \rangle.$$

The thickness of the boundary layer, $\delta_{II} = \pi(\nu/|\omega_1 - \omega_2|)^{1/2}$ and is chosen to be the depth at which the velocity is opposite to that at the surface. This δ_{II} width is used to estimate the fluid heat flux back in Section 1.3. Because the fluid does not rotate as a rigid body with respect to the crystal, we approximate the radial velocity of the fluid to be a fixed proportion of its rigid value so that $v \simeq \gamma r |\omega_1 - \omega_2|$ with $\gamma \simeq 0.05$. To obtain the velocity entering the Ekman layer we take v to be the radial speed of the fluid at a radius of twice the depth of the Ekman layer so that $r \simeq 2\delta_{II}$. This gives $v_{o,II} \simeq 2\pi\gamma(\nu|\omega_1 - \omega_2|)^{1/2}$. By the structure of the Ekman layer, the core velocity, $v_{i,II}$ at $z = -\delta_{II}$ is the same as $v_{o,II}$ except in the opposite direction. As for the flux, this is simply $Q_{II} = \pi l_r^2 v_{o,II} \simeq 2\pi^2 \gamma l_r^2 (\nu|\omega_1 - \omega_2|)^{1/2}$. For the typical rotation rates, 1-10 rpm, one finds that $v_{i,II} = v_{o,II} \simeq 0.2$ mm s^{-1} and $Q_{II} = 0.65$ ml s^{-1}.

This leaves the transient spiral structure. It is expected that this is a result of the fluid entering the Ekman layer having a velocity that far exceeds the speed at the core region of the buoyancy driven cell. Comparing these two velocities gives the expression

$$\frac{\alpha^2}{\pi^2 \gamma^2 \nu} \ll |\omega_1 - \omega_2| \frac{l_r^4}{R_c^2}$$

which indicates that this structure should appear at large rates of rotation. For the values indicated in Table 1.1 one would require $|\omega_1 - \omega_2| \gg 28$ Hz.

1.9   Shape of the Meniscus

The shape of the melt/gas interface, $f_l(r, t)$, is determined by the Laplace-Young equation which describes the equilibrium configuration of a curved liquid surface under the effect of a gravitational field. For cylindrical growth of a crystal the radius of the crystal, l_r, changes according to the expression

$$\frac{dl_r}{dt} = \left(v_p - \frac{dh_r}{dt} \right) \tan(\theta - \theta_o) \tag{1.22}$$

where θ_o is the equilibrium contact angle of the surface with the vertical tangent at the triple point, θ is the current contact angle, v_p is the pull rate and dh_r/dt is rate of change of the crystal height at the outer edge of the crystal. Since the crucible is rotating, the shape of the meniscus and therefore the height of the triple point above the surface $z = 0$ will be affected by this rotation.

Suppose that the fluid velocity is zero so that there are no coriolis effects and the steady state pressure satisfies

$$-\frac{1}{\rho}\nabla P = \nabla \left(gz - \frac{1}{2}\omega^2 r^2 \right)$$

where $\rho \simeq \rho_l$ is difference in density between the liquid and gas phases and where we have taken a rotation rate of $\omega = \omega \hat{\mathbf{k}}$. In addition, the pressure drop across the melt surface, $z = f_l$, is determined by the surface tension, σ_l by

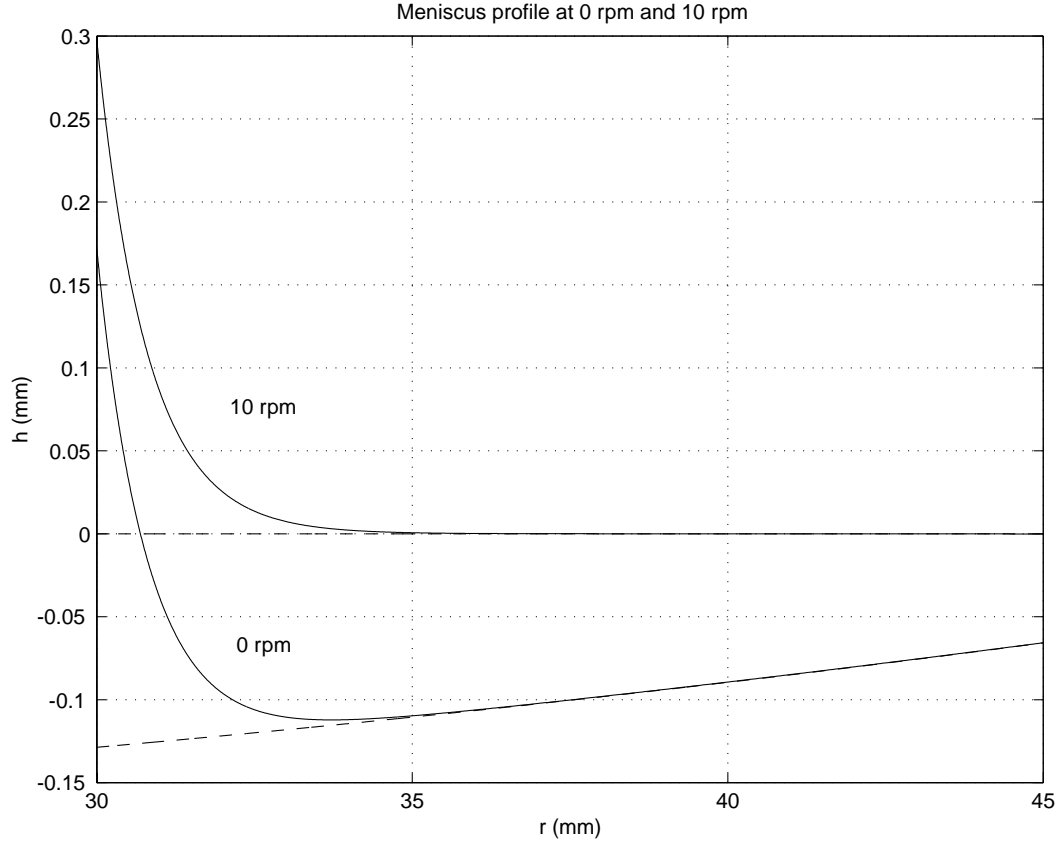$$P = P_o - \sigma\kappa = P_o - \sigma_l \nabla \cdot \left[\frac{\nabla f_l}{(1 + |\nabla f_l|^2)^{1/2}} \right]$$

Figure 1.12: Menisucus profile for the melt/gas interface, $f_l(r,t)$ for no rotation and at 10 rpm.

where κ is the curvature of the free surface.

Setting $f_l = h(r)$, combining these two expressions, and denoting derivatives with respect to r with dots one obtains

$$-\frac{1}{\rho}\nabla P = g\dot{h} - \omega^2 r - \frac{\sigma}{\rho}\frac{d}{dr}\left[\frac{1}{r}\frac{d}{dr}\left(\frac{r\dot{h}}{(1+|\dot{h}|^2)^{1/2}}\right)\right] = 0.$$

Letting $r = ar^*$, $h = ah^*$ with $a^2 = \sigma_l/\rho_l g$ and then dropping the stars gives the nonlinear second order ODE

$$\ddot{h} + \frac{\dot{h}}{r}(1+\dot{h}^2) - \left[h - \frac{a\omega^2}{4g}(2r^2 - R_c^2)\right] = 0, \qquad l_r/a \leq r \leq R_c/a$$

where $\dot{h}(l_r/a) = -\cot(\theta_o)$ and $h(l_r/a)$ is chosen so that

$$\lim_{r\to\infty}\left[h(r) - \frac{a\omega^2}{4g}(2r^2 - R_c^2)\right] = 0$$

and at large radii $h(r)$ approaches the parabolic surface due to the rotation of the crucible.

For InSb, $\sigma_l = 0.434$ J m^{-2}, $\rho_l = 6.47 \times 10^4$ kg m^{-3} and $\theta_o = 69^o$. Figure 1.12 illustrates the meniscus profile for two cases: no rotation and for a rotation rate of 10 rpm. In both of these cases the crystal radius, $l_r = 3$ cm and $R_c = 8$ cm. Increasing the rotation rate drops the height of the triple point.

1.10 A Model for the Melt Height

Up to this point we have taken the coordinate system to be fixed at the crystal/melt interface so that the pulling speed v_p is the sum of the crystal pull rate and the rate at which the fluid level drops in the crucible. In this
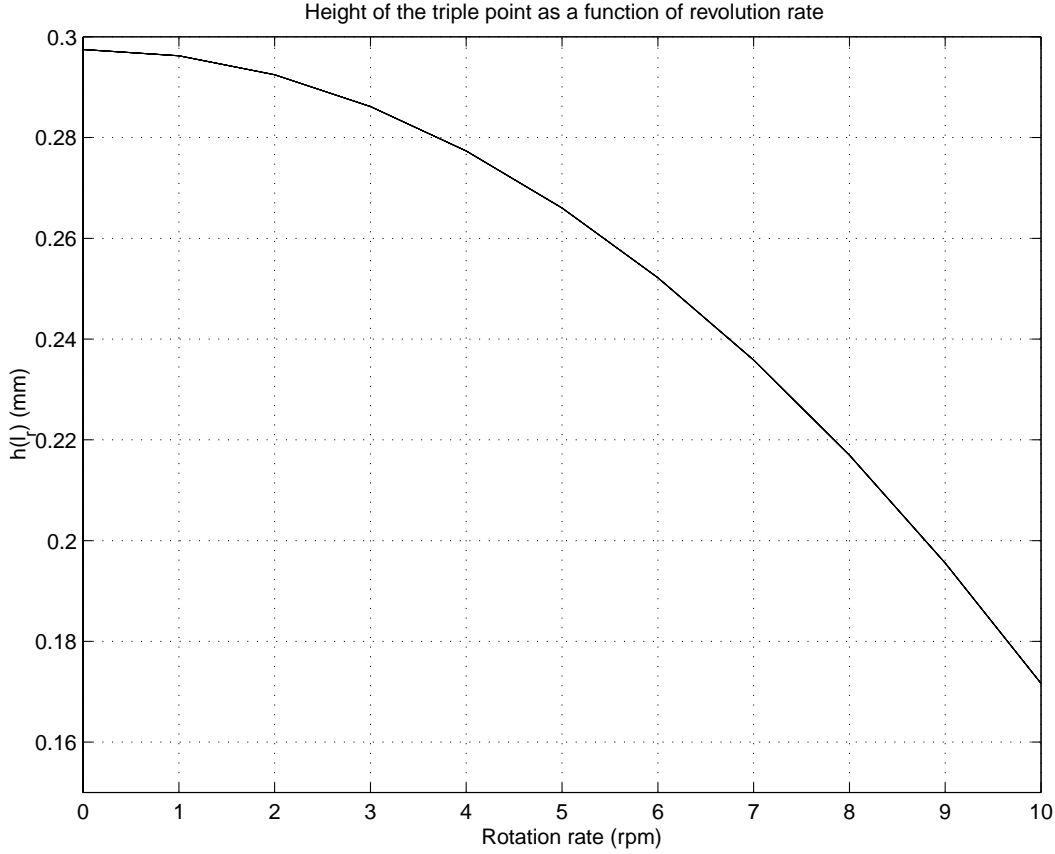
Figure 1.13: Position of the triple point as a function of the rotation rate.

section we will determine the proportion of effective pulling rate that is due to the dropping level of the fluid.

At any time t the mass of the fluid that leaves the crucible must equal the mass that is incorporated into the crystal. That is,

$$\rho_l \frac{\partial V_l}{\partial t} = 2\pi \rho_s \int_0^{R(t)} \left(\frac{\partial S}{\partial t} - v_p \right) r \, dr \tag{1.23}$$

where $R(t)$ is the radius of the crystal at time t and S is the location of the crystal/melt interface. For V_l we assume that the crucible is a hemisphere of radius R_c so that

$$V_l = \pi \left(\frac{2}{3} R_c^3 + S R_c^2 - \frac{1}{3} S^3 \right) \tag{1.24}$$

where $-R_c \leq S(t) \leq 0$. By assuming that the interface is essentially flat $\partial S / \partial r \simeq 0$, expressions (1.23) and (1.24) combine to give

$$\frac{\partial S}{\partial t} = \frac{v_p}{1 - \dfrac{\rho_l}{\rho_s} \dfrac{(R_c^2 - S^2)}{R^2(t)}} \tag{1.25}$$

with $S(0) = 0$ if one starts with an initially full crucible. Expression (1.25) provides an exact solution for the height of the melt surface and can be used to accurately determine the appropriate rate at which to move the crucible. Based on the geometry $t \leq t_c$ where t_c is the time at which the crystal comes in contact with the crucible, $S^2(t_c) + R^2(t_c) = R_c^2$. Consequently, the slope in expression (1.25), $\partial S / \partial t \geq v_p / (1 - \rho_l / \rho_s)$.

When the crystal radius is constant, (1.25) can be integrated to give a cubic equation for S but in general we take $R(t) = l_r + v_p t \tan \varphi$ where $2\varphi \simeq 4^o$ is the growth angle. Figure 1.14 illustrates the height of the surface and
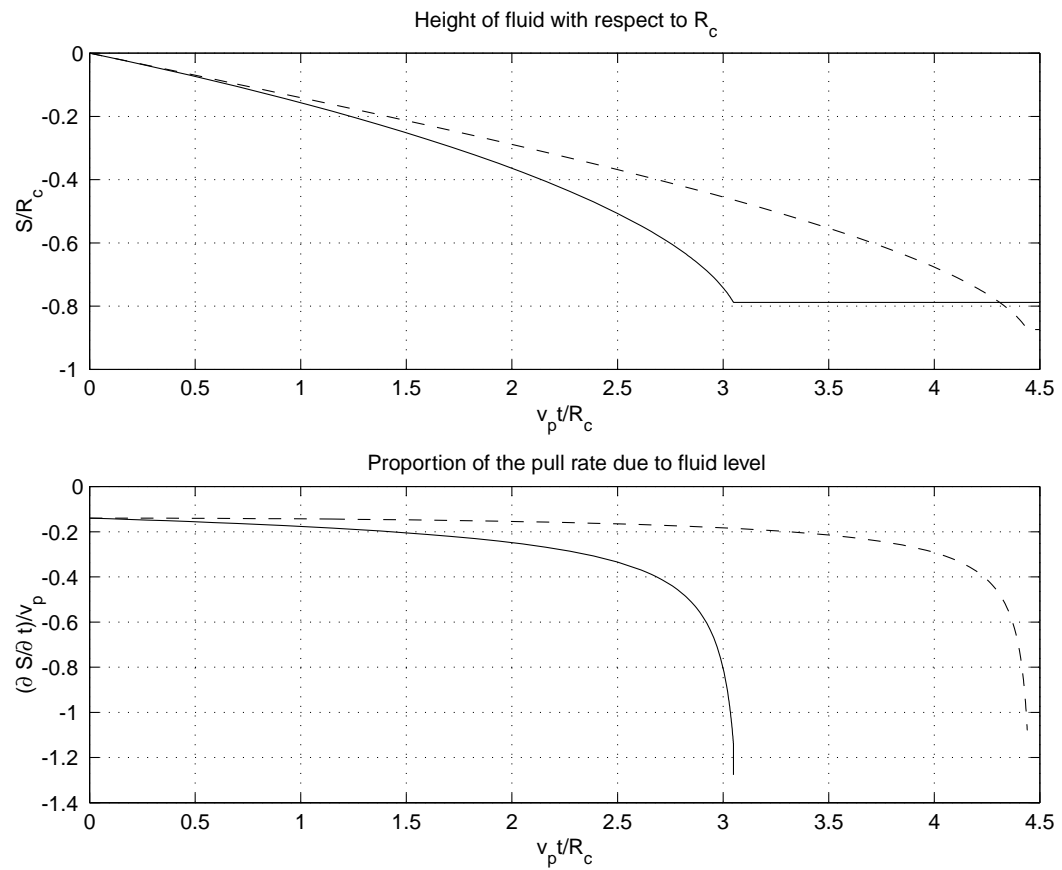
Figure 1.14: The height of the fluid and the proportion of the effective pull rate due to the falling fluid as a function of the non dimensionalized time. The solid line corresponds to $\varphi = 2^o$ while the dashed line is the case of a constant radius, $\varphi = 0$.

the proportion of the effective pull rate due to the falling liquid state for $\varphi = 0$ (constant radius) and $\varphi = 8^o$. For the constant radius case the rate at which the fluid falls is essentially constant until the height of the fluid reaches about $-0.75R_c$. Over this region about 20% of the effective pull rate is due to the falling fluid. As the level drops further, the rate of the falling fluid becomes the dominant effect. When $\varphi = 2^o$ the growing time is reduced since the crystal reaches the sides of the crucible much earlier. However the same behaviour is observed except that the fluid accounts for about 30% of the effective pull rate and this linear behaviour extends for a shorter time period.

1.11   Conclusion

The main purpose of this work was to understand the growing process of InSb with the ultimate hope of growing large radius crystals. Analysing the temperature distribution within the crystal allowed us to estimate the growing rate by solving the Stefan problem. However, this relied on a very crude estimate for the heat flux from the melt. Despite this drawback, it was noticed that the growth rate of the crystal/melt interface is larger at the periphery of the crystal and that the temperature gradients are largest near the triple point. The temperature distribution was used to calculate the von Mises stress. Calculation of the stress is essentially a post processing analysis but could in principle incorporated into a feedback control system used to produce the crystal. One question that has not been addressed is whether or not there exists temperature distributions that produce less von Mises stress. Moreover, if such temperature profiles exist, what changes in the geometry of the growing environment are required?

Another interesting problem is that of the fluid flows. Some heuristic analysis was performed but this appears to be a finely balanced system between the Ekman pumping and the buoyancy flows. Further understanding of this system would be very worthwhile yet complicated by the rotation of the crucible.

The rate which the radius of the crystal grows depends on the effective pull rate and the angle the fluid makes with the extracted crystal. Computing the shape of the meniscus at various rotation rates illustrates that increasing the rotation rate to 10 rpm drops the location of the triple point about one half the height of the nonrotating meniscus. Since the shape of the meniscus determines the location of the triple point and it is near this triple point that much of the thermal stress is generated, inclusion of this effect may be quite important to determining the overall shape of the crystal/melt interface.

Many aspects of the problem of growing InSb crystals were investigated in the hopes of understanding the growing process. Growing larger crystals seems to depend for the most part on controlling the temperature of the surrounding hydrogen gas. Other elements of the growing method were investigated and it is hoped that further work, perhaps on a model that incorporates most of these factors, will yield advances in this method.

Bibliography

[1] Brummell, N., Hart, J.E. & Lopez, J.M. (2000). *On the Flow Induced by Centrifugal Buoyancy in a Differentially-Heated Rotating Cylinder.* Theoretical and Computational Fluid Dynamics, 14, pp 39-54.

[2] Cherepanov, G.P. (1998). *Two-Dimensional Convective Heat/Mass Transfer for Low Prandtl and any Peclet Numbers.* SIAM Journal of Applied Mathematics, 58(3), pp 942-960.

[3] Cook, R.D. (1995). Finite Element Modeling for Stress Analysis. John Wiley & Son Inc.

[4] Crowley, A.B. (1983). *Mathematical Modelling of Heat Flow in Czochralski Crystal Pulling.* Journal of Applied Mathematics, 30, pp 173-189.

[5] Fowkes, N.D. & Hood, M.J. (1997). *Surface tension effects in a wedge.* The Quarterly Journal of Mechanics and Applied Mathematics, 51(4), pp 553-561.

[6] Fowler, A.C. (1997). Mathematical Models in the Applied Sciences. Cambridge Texts in Applied Mathematics. Cambridge University Press.

[7] Hoffmann, K.A. & Chiang, S.T. (2000). Computational Fluid Dynamics for Engineers, Volume 1. www.EESbooks.com.

[8] Jordan, A.S., Caruso, R. & von Neida, A.R. (1979). *A Thermoelastic Analysis of Dislocation Generation in Pulled GaAs Crystals.* The Bell System Technical Journal, 59(4), pp 593-637.

[9] Kusaka, Y. & Tani, A. (1999). *On the Classical Solvability of the Stefan Problem in a Viscous Incompressible Fluid Flow.* SIAM Journal of Mathematics, 30(3), pp 584-602.

[10] Lienhard, H.L. (1987). A Heat Transfer Textbook, (Second Ed.). Prentice-Hall Inc.

[11] Singh, A.K., Pardeshi, R. & Basu, B. (2001). *Modelling of convection during solidifcation of metal and alloys.* Sādhanā, 26(1-2), pp 139-162.

[12] Stewart, R.H. (2002). Introduction to Physical Oceanography. Online textbook.

[13] Talmage, G., Shyru, S.-H., Lopez, J.M. & Walker, J.S. (2000). *Inertial effects in the rotationally driven melt motion during the Czochralski growth of silicon crystals with a strong axial magnetic field.* Zeitschrift für angewandte Mathematik und Physik, 51, pp 267-289.

[14] Wang, Y., Regel, L.L. & Wilcox, W.R. (2001). *Steady state detached solidification of water at zero gravity.* Journal of Crystal Growth, 226, pp 430-435.

[15] Zhang, Z.-C., Yu, S.T.J., Chang, S.-C. & Jorgenson, P.C.E. (2001). *Calculations of Low-Mach-Number Viscous Flows without Preconditioning by the Space-Time CE/SE Method.* Computational Fluid Dynamics 2000. Springer-Verlag, pp 127-132.